

LETTER TO THE EDITOR

Exchange–correlation potential for Current Density Functional Theory of frequency dependent linear response

S Conti, R Nifosì and M P Tosi

INFN and Classe di Scienze, Scuola Normale Superiore, Piazza dei Cavalieri, I-56126 Pisa, Italy

Abstract. The dynamical, long–wavelength longitudinal and transverse exchange–correlation potentials for a homogeneous electron gas are evaluated in a microscopic model based on an approximate decoupling of the equation of motion for the current–current response function. The transverse spectrum turns out to be very similar to the longitudinal one. We obtain evidence for a strong spectral structure near twice the plasma frequency due to a two–plasmon threshold for two–pair excitations, which may be observable in inelastic scattering experiments. Our results give the entire input needed to implement the Time–Dependent Current Density Functional Theory scheme recently developed by G. Vignale and W. Kohn [Phys. Rev. Lett. **77**, 2037 (1996)] and are fitted to analytic functions to facilitate such applications.

PACS numbers: 71.45Gm, 36.40+d, 78.30.Fs, 73.20.Mf

The Time–Dependent Density Functional Theory (TD–DFT) of Runge and Gross [1] in principle allows the study of dynamical properties of interacting many–particle systems, which are not addressed by static DFT. The adiabatic local density approximation (ALDA) [2] has enabled successful application of the theory in the low–frequency limit. The search for a local dynamical approximation to the exchange–correlation (xc) potential has been frustrated by the appearance of various inconsistencies [3, 4, 5], which can be tracked down to the non–existence of a gradient expansion for the frequency–dependent xc potential in terms of the density alone.

Recently Vignale and Kohn (VK) have shown how a local approximation for the xc vector potential $\mathbf{a}^{xc}(\mathbf{r}, \omega)$ can be obtained within linearized Current Density Functional Theory [6, 7]. They prove that for slowly varying densities known symmetries and conservation laws allow one to express $\mathbf{a}^{xc}(\mathbf{r}, \omega)$ exactly in terms of the long–wavelength xc potentials $f_{xc}^{L,T}(\omega)$ for a homogeneous electron gas,

$$\begin{aligned} \mathbf{a}_i^{xc}(\mathbf{r}, \omega) = & -\frac{1}{\omega^2} \{ \partial_i [f_{xc}^L \nabla \cdot (n_0 \mathbf{v}) - \delta f_{xc}^L \mathbf{v} \cdot \nabla n_0] + \delta f_{xc}^L (\partial_i n_0) \nabla \cdot \mathbf{v} \\ & + f_{xc}^T [-n_0 (\nabla \times \nabla \times \mathbf{v})_i + 2(\partial_j \mathbf{v}_i + \partial_i \mathbf{v}_j) \partial_j n_0 - 4(\partial_i n_0) \nabla \cdot \mathbf{v}] \\ & + n_0 ((\partial_j f_{xc}^T) (\partial_i \mathbf{v}_j + \partial_j \mathbf{v}_i) - 2(\partial_i f_{xc}^T) \nabla \cdot \mathbf{v}) \} . \end{aligned} \quad (1)$$

Here, $n_0(\mathbf{r})$ is the unperturbed ground–state density, $\mathbf{v}(\mathbf{r}, \omega) = \mathbf{j}_1(\mathbf{r}, \omega)/n_0(\mathbf{r})$ is the local velocity and $\delta f_{xc}^L(\omega, n) = f_{xc}^L(\omega, n) - f_{xc}^L(0, n)$. The potentials $f_{xc}^{L,T}$, which are functions of ω and of the local density $n_0(\mathbf{r})$, are defined as the $k \rightarrow 0$ limit of

$$f_{xc}^{L,T}(k, \omega) = \frac{\omega^2}{k^2} \left\{ \frac{1}{\chi_{L,T}^0(k, \omega) + \rho/m} - \frac{1}{\chi_{L,T}(k, \omega) + \rho/m} \right\} - v_{L,T} \quad (2)$$

where $\chi_{L(T)}$ is the current–current longitudinal (transverse) response function of the homogeneous system at density $\rho = n_0(\mathbf{r})$, $\chi_{L(T)}^0$ is the equivalent ideal–gas quantity, $v_L = 4\pi e^2/k^2$ and $v_T = 0$.

The quest for a frequency–dependent local field factor $G(k, \omega) = -f_{xc}^L(k, \omega)/v_L$ for the density–density response is a long–lasting problem in electron gas theory [8, 9, 10, 11, 12, 13, 14, 15]. Its asymptotic behaviours are known from sum rule arguments [8, 9] and from second–order perturbative expansions [11, 12, 13], and a smooth interpolation scheme was proposed by Gross and Kohn [9, 10]. A fully microscopic result, derived from an approximate treatment of two–pair excitations, was obtained by Böhm *et al* [16, 17] using an expression first derived by Hasegawa and Watabe [11]. The longitudinal component of the current–current xc potential $f_{xc}^L(\omega)$ can be obtained from such results, but no sensible approximations have been proposed for the transverse component, preventing implementation of the Vignale–Kohn theory.

In this letter we develop a full treatment of the two–pair excitation spectrum, including its transverse component. Our results give the entire input necessary to use the VK expression.

The xc potential can be obtained within the equation of motion formalism. A general response function is defined as

$$\ll A; B \gg_\omega = -i \int_0^\infty dt e^{i(\omega + i\epsilon)t} \langle [A(t), B(0)] \rangle \quad (3)$$

where $A(t) = e^{iHt} A e^{-iHt}$ and $\langle \dots \rangle$ denotes ground state expectation values. The current–current response $\chi_{ij}(k, \omega) = \ll \mathbf{j}_{\mathbf{k}}^i; \mathbf{j}_{-\mathbf{k}}^j \gg$ satisfies the equation of motion

$$\chi_{ij}(k, \omega) = \frac{1}{\omega^2} \langle [\mathbf{j}_{\mathbf{k}}^i, H], \mathbf{j}_{-\mathbf{k}}^j \rangle > -\frac{1}{\omega^2} \ll [\mathbf{j}_{\mathbf{k}}^i, H]; [\mathbf{j}_{-\mathbf{k}}^j, H] \gg_\omega . \quad (4)$$

The last term yields four–point response functions $\ll AB; CD \gg_\omega$ involving $\rho_{\mathbf{k}}$ and $\mathbf{j}_{\mathbf{k}}$ operators and can be approximately decoupled by an RPA–like scheme:

$$\begin{aligned} \mathbf{Im} \ll AB; CD \gg_\omega &\simeq - \int_0^\omega \frac{d\omega'}{\pi} [\mathbf{Im} \ll A; C \gg_{\omega'} \mathbf{Im} \ll B; D \gg_{\omega-\omega'} \\ &+ \mathbf{Im} \ll A; D \gg_{\omega'} \mathbf{Im} \ll B; C \gg_{\omega-\omega'}]. \end{aligned} \quad (5)$$

Such a decoupling includes by construction two–pair processes, which are the lowest order processes with non–zero spectral strength in the relevant region of the (k, ω) plane. Perturbative approaches evaluate the LHS of equation (5) for an ideal gas and obtain a spectrum restricted to single pair excitations, which is essentially equivalent to the one obtained by using non–interacting response functions in the RHS (the difference lies in exchange processes, as discussed below). We intend to include the effect of plasmons and therefore use RPA response functions in the RHS.

Quite lengthy calculations lead in this approach to the following result for the xc potentials $f_{xc}^{L,T}(\omega)$ in terms of the response functions introduced in equation (2):

$$\begin{aligned} \mathbf{Im} f_{xc}^{L,T}(\omega) &= - \int_0^\omega \frac{d\omega'}{\pi} \int \frac{d^3q}{(2\pi)^3 \rho^2} v_q^2 \frac{q^2}{(\omega - \omega')^2} \mathbf{Im} \chi_L(q, \omega - \omega') \\ &\times \left[a_{L,T} \frac{q^2}{\omega'^2} \mathbf{Im} \chi_L(q, \omega') + b_{L,T} \frac{q^2}{\omega^2} \mathbf{Im} \chi_T(q, \omega') \right] \end{aligned} \quad (6)$$

with $a_L = 23/30$, $a_T = 8/15$, $b_L = 8/15$ and $b_T = 2/5$. The expression for the longitudinal part is equivalent to the one obtained by Hasegawa and Watabe [11] by

Table 1. Exact limiting behaviours of $f_{xc}^{L,T}(\omega)$ from the Monte Carlo equation of state, in units of $2\omega_{pl}/\rho$, and best fit parameters for $\mathbf{Im} f_{xc}^L$ according to (12).

r_s	$f_{xc}^L(0)$	$f_{xc}^L(\infty)$	$f_{xc}^T(\infty)$	β	$10^2 c_0$	$10^2 c_1$	ω_1	ω_2	d_0	$10^2 d_1$
0.5	-0.04246	-0.01794	0.0177	1.87	0.175	0.694	1.75	-3.59	0.173	5.72
1	-0.0611	-0.0216	0.0284	1.48	0.421	1.76	0.982	-1.45	0.291	9.38
2	-0.0891	-0.0252	0.0457	1.22	0.895	3.87	0.347	0.181	0.49	13.2
3	-0.1119	-0.0280	0.0600	1.1	1.29	6.09	0.143	0.693	0.664	16.7
4	-0.1320	-0.0308	0.0724	1.02	1.65	7.87	-0.143	1.33	0.824	17
5	-0.1503	-0.0338	0.0835	0.955	1.94	9.82	-0.27	1.61	0.974	18.3
6	-0.1674	-0.0370	0.0935	0.899	2.22	11.6	-0.361	1.82	1.12	19.3
10	-0.2276	-0.0518	0.1267	0.698	3.11	17.9	-0.565	2.27	1.64	22.1
15	-0.2917	-0.0725	0.1587	0.474	3.94	24.2	-0.69	2.54	2.22	23.9
20	-0.3483	-0.0939	0.1847	0.259	5.54	24.7	-0.808	2.78	2.75	22.8

diagrammatic means, and similar to the one obtained by Neilson *et al.* [15] (see the discussion in [16]). The result for the transverse component is new.

The real part of f_{xc} can be obtained via the Kramers–Kronig relations, namely

$$\mathbf{Re} f_{xc}(\omega) = \mathbf{Re} f_{xc}(\infty) + \frac{1}{\pi} \int_{-\infty}^{+\infty} d\omega' \frac{\mathbf{Im} f_{xc}(\omega')}{\omega' - \omega}. \quad (7)$$

The first term in the RHS of equation (4) fixes the high-frequency limit

$$f_{xc}^{L,T}(\omega = \infty) = \frac{1}{2\rho} [d_{L,T}(\langle ke \rangle - \langle ke \rangle^0) + e_{L,T} \langle pe \rangle] \quad (8)$$

with $d_L = 4$, $d_T = 4/3$, $e_L = 8/15$ and $e_T = -4/15$. The average kinetic and potential energies $\langle ke \rangle$ and $\langle pe \rangle$ can be obtained from the Monte Carlo equation of state [18], as can the compressibility K_T which fixes the longitudinal static limit

$$\lim_{k \rightarrow 0} \lim_{\omega \rightarrow 0} f_{xc}^L(k, \omega) = \frac{1}{\rho^2} \left(\frac{1}{K_T} - \frac{1}{K_T^0} \right). \quad (9)$$

In the above equations, $\langle ke \rangle^0$ and K_T^0 denote ideal gas results. The asymptotic values of $f_{xc}^{L,T}$ are listed in Table 1. We remark that there is no proof that the order of limits in equation (9) can be safely interchanged nor in general that $f_{xc}^L(k, \omega)$ is a continuous function in the limit $(k, \omega) \rightarrow (0, 0)$. Indeed, there are arguments which indicate a small discontinuity [19]. In view of (i) the small estimated discontinuity, (ii) the uncertainty in its precise value and (iii) the appeal of a theory which reduces continuously to LDA as $\omega \rightarrow 0$, we prefer to enforce continuity as explained below.

The above approximation neglects exchange processes, which in perturbative treatments reduce the total two-pair spectral weight by a factor of 2 if $\omega \gg \varepsilon_F$, ε_F being the Fermi energy. We approximately include exchange by multiplying $\mathbf{Im} f_{xc}^L$ by the phenomenological factor

$$g_x(\omega) = \frac{\beta + 0.5\omega/2\varepsilon_F}{1 + \omega/2\varepsilon_F}, \quad (10)$$

where the parameter β is used to enforce continuity at $k = \omega = 0$ and turns out to be close to 1 at metallic densities (see Table 1). For consistency we use the same factor $g_x(\omega)$ in the transverse component. Our final high-frequency result is

$$\mathbf{Im} f_{xc}^{L,T}(\omega \rightarrow \infty) = -2c_{L,T} \left(\frac{2Ry}{\omega} \right)^{3/2} a_B^3 Ry \quad (11)$$

where $c_L = 23\pi/15$ and $c_T = 16\pi/15$, in agreement with the result of Glick and Long [13] for the longitudinal term and its extension to the transverse one (unpublished).

Equations (6) could be considered as the $k = 0$ component of a self-consistency condition, but the self-consistent problem cannot be solved since the equations determining the finite- k behaviour of f_{xc} are unknown. We have evaluated equation (6) by using the RPA response functions in the LHS. The imaginary part of the RPA longitudinal susceptibility consists of two separate contributions: the first arises from the broad single-pair continuum, the other from the sharply peaked plasmon excitation. In turn this leads to a structure in $\mathbf{Im}f_{xc}(\omega)$ around twice the plasma frequency (for details see Ref. [16]). As we are neglecting retardation the transverse susceptibility contains only a broad continuum and therefore has larger spectral strength than the longitudinal one at low frequency.

Figures 1 and 2 report our results for the imaginary and real parts of f_{xc} and compare them with the interpolation scheme of Gross and Kohn [9] for the longitudinal term. Both curves reproduce the asymptotic limits (8) and (9) as well as the $\omega^{-3/2}$ high-frequency behaviour, but the behaviours at intermediate frequencies are strikingly different. Our curves for $\mathbf{Re}f_{xc}$ exhibit a sharp minimum around $2\omega_{pl}$, which corresponds to the sharp structure found in $\mathbf{Im}f_{xc}$ at the same frequency. The physical origin lies in the large spectral strength of the plasmon excitation as compared to single-pair excitations, which accumulates most of the spectral strength of two-pair processes near $2\omega_{pl}$. This spectral structure becomes sharper with increasing coupling strength, i.e. with increasing r_s (r_s is defined as $(4\pi\rho a_B^3/3)^{-1/3}$, a_B being the effective Bohr radius). We note that within the accuracy of the present model $f_{xc}^T(\omega = 0)$ is indistinguishable from zero in the entire density range explored here.

Figure 2 shows stronger xc effects in the real part at intermediate frequencies ($\omega \simeq \omega_{pl}$) than in both the $\omega = 0$ and the $\omega = \infty$ limit, at variance from the Gross-Kohn interpolation. Available experimental data on the plasmon dispersion coefficient in alkali metals [20] indicate much stronger deviations from RPA than predicted by existing electron gas theories. Although band-structure effects play a significant role in a quantitative comparison, the dynamic correction indicated by our results improves the agreement with the experimental data.

Figure 3 displays the dynamic structure factor $S(k, \omega) = -(2k^2/\rho\omega^2)\mathbf{Im}\chi_L(k, \omega)$ which is relevant to inelastic scattering experiments. The threshold behaviour at frequency $2\omega_{pl}$ is a clearcut signature of the present results for f_{xc} .

While the detailed shapes of our results are largely approximation-dependent, we do not expect the main qualitative features to be substantially modified in a more refined theory. Both self-consistent SPA results [16] and preliminary calculations with an STLS response function [8] show the same qualitative behaviours at values of r_s where the plasmon dispersion coefficient is positive. A much deeper minimum in $\mathbf{Re}f_{xc}$ is found at negative plasmon dispersion, which in STLS is the case for $r_s > 5$.

We also remark that the shapes of the longitudinal and transverse spectra are very similar. Equation (6) shows that $\mathbf{Im}f_{xc}^T = 16/23 \cdot \mathbf{Im}f_{xc}^L$ for $\omega \gg \omega_{pl}$ whereas $\mathbf{Im}f_{xc}^T = 3/4 \cdot \mathbf{Im}f_{xc}^L$ for $\omega \ll \omega_{pl}$. In fact, the transverse spectrum is rather accurately reproduced at all frequencies by setting $\mathbf{Im}f_{xc}^T(\omega) \simeq 0.72 \cdot \mathbf{Im}f_{xc}^L(\omega)$, whereas for the real part there is an additional shift due to the different $\omega = \infty$ value.

Our numerical results for $\mathbf{Im}f_{xc}^L(\omega)$ can be accurately reproduced by the expression

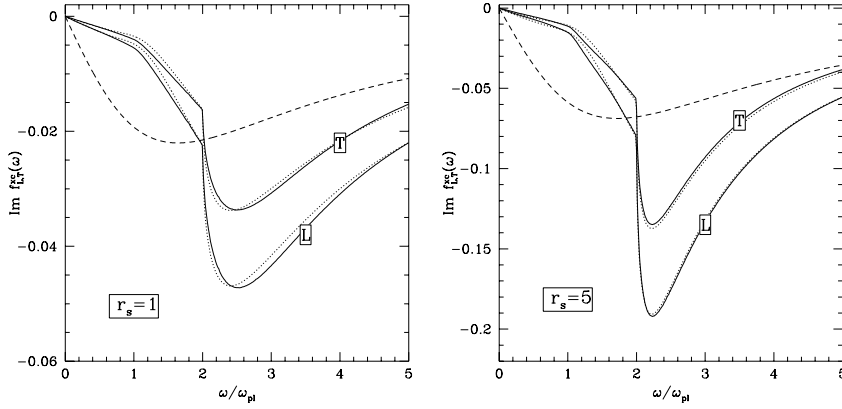


Figure 1. Imaginary parts of $f_{xc}^L(\omega)$ and $f_{xc}^T(\omega)$ in units of $2\omega_{pl}/\rho$, as functions of ω/ω_{pl} at $r_s = 1$ (left panel) and $r_s = 5$ (right panel). The present results (full curves) are compared with the Gross-Kohn interpolation for the longitudinal component (dashed curves) and with the fit discussed in the text (dotted curves).

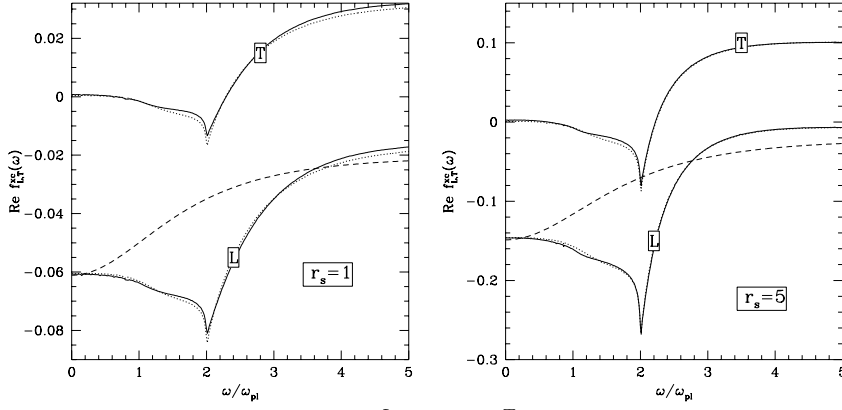


Figure 2. Real parts of $f_{xc}^L(\omega)$ and $f_{xc}^T(\omega)$ (full curves), in units of $2\omega_{pl}/\rho$, as functions of ω/ω_{pl} at $r_s = 1$ (left panel) and $r_s = 5$ (right panel). The meaning of the other curves is as in Figure 1.

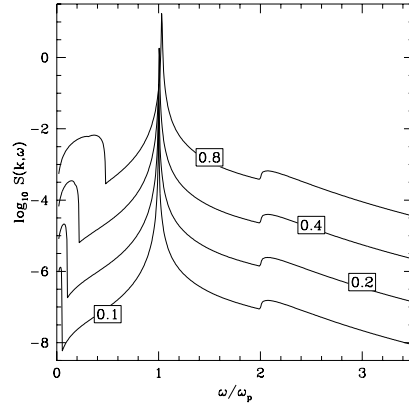


Figure 3. Dynamic structure factor $S(k, \omega)$ at $r_s = 5$ as a function of ω/ω_{pl} at various values of $kr_s a_B$ on a semilogarithmic scale.

$$\mathbf{Im}f_{xc}^L(\omega) = -g_x(\omega) \begin{cases} c_0\omega + c_1 \frac{\omega - 1}{e^{(7/\omega)-5} + 1} & (\omega < 2) \\ \frac{d_0\sqrt{\omega - 2} + d_1}{\omega(\omega - \omega_1\sqrt{\omega} - \omega_2)} & (\omega > 2) \end{cases} \quad (12)$$

where ω is in units of ω_{pl} , f_{xc}^L in units of $2\omega_{pl}/\rho$. The fit parameters given in Table 1 were obtained by imposing (i) continuity at $\omega = 2\omega_{pl}$, (ii) conservation of the normalization $\int \mathbf{Im}f_{xc}d\omega/\omega$ and (iii) the asymptotic behaviour given by equation (11). The remaining three parameters were fitted to the numerical data. The real part can be obtained from the Kramers–Kronig relation and the high–frequency values given in Table 1; the low–frequency longitudinal values from the same Table can be used for a check. The good quality of the resulting fits is shown in Figures 1 and 2.

In summary, we have presented a microscopic model for the longitudinal and transverse xc potentials of the 3D homogeneous electron gas. We have given numerical evaluations yielding results which are significantly different from previous interpolation schemes and compatible with experimental data on the plasmon dispersion coefficient. Our results have been fitted to analytic expressions and provide all the input needed for TD–DFT computations in the linearized long–wavelength regime.

Acknowledgments

We gratefully acknowledge very useful discussions with Professor G. Vignale.

References

- [1] Runge E and Gross E K U 1984 *Phys. Rev. Lett.* **52** 997
- [2] Zangwill A and Soven P 1980 *Phys. Rev. Lett.* **45** 204
- [3] Dobson J 1994 *Phys. Rev. Lett.* **73** 2244
- [4] Vignale G 1995 *Phys. Rev. Lett.* **74** 3233
- [5] Gross E K U, Dobson J F and Petersilka M 1996 in *Density Functional Theory Topics in Current Chemistry* edited by Nalewajski R F (Berlin: Springer)
- [6] Vignale G and Kohn W 1996 *Phys. Rev. Lett.* **77** 2037
- [7] Vignale G and Kohn W 1997 in *Electronic Density Functional Theory* edited by Dobson J, Das M P and Vignale G (New York: Plenum Press)
- [8] Singwi K S and Tosi M P 1981 *Solid State Phys.* **36** 177
- [9] Gross E K U and Kohn W 1985 *Phys. Rev. Lett.* **55** 2850; *ibid.* **57**, 923 (1986)
- [10] Iwamoto N and Gross E K U 1987 *Phys. Rev. B* **35** 3003
- [11] Hasegawa M and Watabe M 1969 *J. Phys. Soc. Jpn.* **27** 1393
- [12] Holas A and Singwi K S 1989 *Phys. Rev. B* **40** 158
- [13] Glick A J and Long W F 1971 *Phys. Rev. B* **4** 3455
- [14] Richardson C F and Ashcroft N W 1994 *Phys. Rev. B* **50** 8170
- [15] Neilson D, Swierkowski L, Sjölander A and Szymanski J 1991 *Phys. Rev. B* **44** 6291
- [16] Böhm H M, Conti S and Tosi M P 1996 *J. Phys.: Condens. Matter* **8** 781
- [17] Conti S, Böhm H M and Tosi M P 1996 *Phys. Stat. Sol (b)* **193** K11
- [18] Ceperley D M and Alder B J 1980 *Phys. Rev. Lett.* **45** 566; Vosko S H, Wilk L and Nusair M 1980 *Can. J. Phys.* **58**, 1200
- [19] The Landau theory of Fermi liquids allows one to express $\lim_{\omega \rightarrow 0} \lim_{k \rightarrow 0} f_{xc}^L(k, \omega)$ and $\lim_{k \rightarrow 0} \lim_{\omega \rightarrow 0} f_{xc}^L(k, \omega)$ in terms of the Landau parameters F_0 , F_1 and F_2 . Preliminary numerical evaluations indicate a 10–20% discontinuity at metallic densities (S. Conti and G. Vignale, unpublished)
- [20] vom Felde A, Sprösser-Prou J and Fink J 1989 *Phys. Rev. B* **40** 10181